Entanglement entropy scaling in critical phases of one-dimensional quasiperiodic systems

Miguel Gonçalves
CeFEMA-LaPMET, Departamento de Física, Instituto Superior Técnico, Universidade de Lisboa, Avenida Rovisco Pais, 1049-001 Lisboa, Portugal
and Centro de Física das Universidades do Minho e Porto, Departamento de Física e Astronomia, Faculdade de Ciências, Universidade do Porto, 4169-007 Porto, Portugal

(Received 9 January 2024; revised 20 February 2024; accepted 21 February 2024; published 7 March 2024)

We study the scaling of the entanglement entropy in different classes of one-dimensional fermionic quasiperiodic systems with and without pairing, focusing on multifractal critical points/phases. We find that the entanglement entropy scales logarithmically with the subsystem size N_A with a proportionality coefficient $\mathcal{C}$, as in homogeneous critical points, apart from possible additional small oscillations. In the absence of pairing, we find that the entanglement entropy coefficient $\mathcal{C}$ is nonuniversal and depends significantly and nontrivially both on the model parameters and electron filling, in multifractal critical points. In some of these points, $\mathcal{C}$ can take values close to the homogeneous (or ballistic) system, although it typically takes smaller values. We find a close relation between the behavior of the entanglement entropy and the small-q (long-wavelength) dependence of the momentum structure factor $\mathcal{S}(q)$. $\mathcal{S}(q)$ increases linearly with q as in the homogeneous case, with a slope that grows with $\mathcal{C}$. In the presence of pairing, we find that even the addition of small anomalous terms affects very significantly the scaling of the entanglement entropy compared to the unpaired case. In particular, we focused on topological phase transitions for which the gap closes with either extended or critical multifractal states. In the former case, the scaling of the entanglement entropy mirrors the behavior observed at the critical points of the homogeneous Kitaev chain, while in the latter, it shows only slight deviations arising at small length scales. In contrast with the unpaired case, we always observe $\mathcal{C} \approx 1/6$ for different critical points, the known value for the homogeneous Kitaev chain with periodic boundary conditions.

DOI: 10.1103/PhysRevB.109.104202

I. INTRODUCTION

The study of entanglement in many-body systems has been a great example of success where remarkable new insights were attained by applying concepts from quantum information theory to condensed matter systems. Among them, the universal scaling of the entanglement entropy in conformal critical points of one-dimensional (1D) systems stands out [1–4]. At these critical 1D systems, the entanglement entropy of a finite subsystem of an infinite system with N_A sites, scales as $S = \mathcal{C}\log(N_A) + \text{cte}$, where $\mathcal{C} = c/3$ for systems with periodic boundary conditions (we refer below to systems with periodic boundaries unless otherwise stated) and c is the universal central charge of the corresponding conformal field theory. For a free fermion chain (that can be mapped to the XX model, through a Jordan-Wigner transformation), $c = 1$. However, at the critical points of the topological phase transitions in the Kitaev chain (or XY model), we have $c = 1/2$. In the presence of a gap, the entanglement entropy also scales logarithmically up to a length scale of the order of the inverse energy gap, above which it saturates. Given the universality of the entanglement entropy scaling, it does not depend on model details for a group of models that are all described by the same low-energy conformal field theory. This includes the addition of inhomogeneities such as disorder, which can therefore still lead to universal behavior [5–11].

Other very interesting inhomogeneous systems for which entanglement has been less studied are quasiperiodic systems. These systems offer a wide range of exciting physics, from interesting localization properties [12–24] to topological features and edge physics [25–27]. Interest in quasiperiodic systems has been recently renewed due to progress in experiments in optical lattices [13,15,16,28,29] and metamaterials [14,22,25,27,30], and the increased focus on moiré systems [31,32].

In one dimension, quasiperiodic systems host rich localization physics, transitions between extended ballistic phases with plane-wave-like eigenstates and localized phases, where the wave function is exponentially localized in real-space [12–16]. At the critical point, the eigenstates are multifractal both in real and momentum space. For some systems, non-fine-tuned phases with multifractal eigenstates can arise [33–40]. The entanglement entropy has been previously studied in quasiperiodic systems [41–47]. For the half-filled paradigmatic Aubry-André model [12], it was found to scale logarithmically with subsystem size at the extended phase and critical point, and to saturate in the localized phase at length scales larger than the localization length [43,45,48]. The results in Ref. [42] indicated that the scaling behavior of the entanglement entropy was different in extended and critical points of the Aubry-André model at different fillings. In the extended phase, the entanglement entropy was found to behave as in the homogeneous case, scaling with $\mathcal{C} \approx 1/3$. At the critical point, however, a different coefficient $\mathcal{C} \approx 0.26$ was observed [45]. The entanglement entropy of a generalized Aubry-André model with long-range (power-law decaying)

hoppings was also studied in Ref. [47], at half-filling. For some parameters, it was found that $\mathcal{C} \neq 1/3$ even in the extended phase. In critical phases, $\mathcal{C}$ was always found to be significantly lower. This raises the question on whether extended and critical phases can always be distinguished based on the scaling of the entanglement entropy. Moreover, a lot remains to explore on the behavior of the entanglement entropy in more generic regimes and different critical points and critical phases. In the presence of pairing, the entanglement entropy has not been studied so far on critical points, to our knowledge.

In this work, using numerically exact methods, we study the behavior of the entanglement entropy in different classes of one-dimensional quasiperiodic systems both with and without pairing terms. We focus on multifractal critical points/phases and find that even though the entanglement entropy scales logarithmically with the subsystem size, apart from possible small oscillations, the coefficients $\mathcal{C}$ depend significantly on the model parameters and electron filling in the absence of pairing. In fact, we observe that $\mathcal{C} \approx 1/3$ at some critical points, with the entanglement entropy behaving similarly to the homogeneous case. Interestingly, the scaling of the entanglement entropy is closely related with the long-wavelength (low-energy) behavior of the momentum structure factor $\mathcal{S}(q)$, growing linearly with q, with a slope that increases with $\mathcal{C}$.

To understand the impact of the pairing terms, we studied the quasiperiodic Kitaev chain, focusing on critical points of topological phase transitions. In this case, we found that the entanglement entropy behaves very similarly to the homogeneous Kitaev chain, where $\mathcal{C} = 1/6$, irrespectively of the model parameters. This is true no matter whether extended or multifractal states are present at the critical point, with the most significant deviations from the $\mathcal{C} = 1/6$ behavior only occurring for the latter case, at small length scales.

Our results show that while in the absence of pairing the scaling of the entanglement entropy can vary quite significantly in critical phases and even become very similar to the homogeneous case, the addition of pairing terms, even if small, is highly relevant and the scaling tends to become very similar to the homogeneous Kitaev critical chain at sufficiently large length scales.

II. MODEL AND METHODS

A. Models

We consider the following class of Hamiltonians:

$$\mathcal{H} = -t \sum_n (c_n^\dagger c_{n+1} + c_{n+1}^\dagger c_n) + \sum_n V_n c_n^\dagger c_n + \Delta \sum_n (c_n c_{n+1} + c_{n+1}^\dagger c_n^\dagger), \tag{1}$$

where $c_n^\dagger$ creates an electron at site n and V_n will be considered to be either of the following quasiperiodic potentials: $V_n^{(1)} = V\cos(2\pi\tau n + \phi) - \mu$ and $V_n^{(2)} = \cos(2\pi\tau n + \phi)/[1 + \alpha\cos(2\pi\tau n + \phi)] - \mu$. In the definitions of V_n, τ is an irrational number that we take to be $\tau = (\sqrt{5}-1)/2$, ϕ is a (phase) shift in the quasiperiodic potential and μ is the chemical potential. In what follows, energy will be measured in units of t. We will study three particular cases of the Hamiltonian in Eq. (1): the Aubry-André model ($\Delta = 0$ and $V_n^{(1)}$) [12], the Ganeshan-Pixley-Sarma (GPS) model, with $\Delta = 0$ and $V_n^{(2)}$ [49], and the quasiperiodic Kitaev chain model, $\Delta \neq 0$ with $V_n^{(1)}$. For the GPS model, the localization phase diagram is analytically known, hosting extended, localized and critical phases [39,49]. For the quasiperiodic Kitaev chain, the localization and topological phase diagrams in the (V, Δ) plane have also been explored [33,35,50,51]. In particular, for $\mu = 0$, a topological phase transition between a topological phase with zero-energy majorana modes and a trivial phase takes place. At this critical point there is also a localization transition between phases with critical multifractal eigenstates (topological) and localized eigenstates (trivial).

To simulate finite systems we followed the usual procedure carried out for QPS [52–54]: for each size $N = F_n$, we take τ to be a rational approximant of the inverse of the golden ratio, $\tau = \tau_n = F_{n-1}/F_n$, where F_n is the nth Fibonacci number. Note that in this way the finite system is incommensurate (the system's unit cell for $\tau = \tau_n$ has precisely N sites, the total system size) and we may apply periodic boundary conditions (PBC) without defects.

B. Entanglement entropy and fidelity

We can write the quadratic fermionic Hamiltonian in Eq. (1) in the Nambu representation,

$$\mathcal{H} = \frac{1}{2}\boldsymbol{C}^\dagger \boldsymbol{H}\boldsymbol{C}, \quad \boldsymbol{H} = \begin{pmatrix} \boldsymbol{h} & \boldsymbol{\Delta} \\ \boldsymbol{\Delta}^\dagger & -\boldsymbol{h}^T \end{pmatrix}, \tag{2}$$

where $\boldsymbol{C} = (c_1, \ldots, c_N, c_1^\dagger, \ldots, c_N^\dagger)^T$ is a Nambu vector and

$$\boldsymbol{h} = \begin{pmatrix} V_0 & -t & 0 & \cdots & -t \\ -t & V_1 & -t & \cdots & 0 \\ 0 & -t & \ddots & \cdots & \vdots \\ \vdots & \vdots & \cdots & V_{N-2} & -t \\ -t & 0 & \cdots & -t & V_{N-1} \end{pmatrix}, \tag{3}$$

$$\boldsymbol{\Delta} = \begin{pmatrix} 0 & \Delta & 0 & \cdots & -\Delta \\ -\Delta & 0 & \Delta & \cdots & 0 \\ 0 & -\Delta & \ddots & \cdots & \vdots \\ \vdots & \vdots & \cdots & 0 & \Delta \\ \Delta & 0 & \cdots & -\Delta & 0 \end{pmatrix}, \tag{4}$$

with these matrices satisfying $\boldsymbol{h} = \boldsymbol{h}^\dagger$ and $\boldsymbol{\Delta} = -\boldsymbol{\Delta}^T$. The single-particle correlation matrix can then be defined as $\boldsymbol{\chi} = \mathrm{tr}(Z^{-1}e^{-\beta\mathcal{H}}\boldsymbol{C}\boldsymbol{C}^\dagger) = \mathbb{I} - n_F(\boldsymbol{H})$, where β is the inverse temperature, Z is the partition function, and n_F is the Fermi-Dirac distribution. To compute the entanglement entropy, we consider our subsystem A to contain the first N_A sites of the full chain containing N sites. The entanglement entropy can then be computed as

$$S_A = -\mathrm{Tr}[\boldsymbol{\chi}_A \ln \boldsymbol{\chi}_A], \quad \boldsymbol{\chi}_A = [\boldsymbol{\chi}]_{i,j\in\mathcal{A}\cup(\mathcal{A}+N)}, \tag{5}$$

where i, j are entries of matrix $\boldsymbol{\chi}$, $\mathcal{A}$ is the set of site indexes of subsytem A and $\mathcal{A}+N$ are the indices obtained by summing N to each of the site indices in $\mathcal{A}$.

In what follows, we average the results for the entanglement entropy over random uniformly distributed realizations of phase ϕ, unless otherwise stated. For the calculations in the Aubry-André and GPS models, we also average over random twisted boundary conditions, by closing the boundaries with a phase twist e^{ik} ($k = 0$ for PBC) [18]. We estimate the error bars of the average entanglement entropy through the error of the mean.

For a 1D critical system whose continuum limit is a conformal field theory, we have that [2,3]

$$S = \mathcal{C} \log\left(\frac{N}{\pi}\sin(\pi N_A/N)\right) + C', \tag{6}$$

where N_A is the number of sites in subsystem A, in which case the central charge of the conformal field theory is given by $3\mathcal{C}$, for periodic boundary conditions. For $N_A \ll N$ we therefore have $S = \mathcal{C}\log N_A$. For the homogeneous fermionic chain with no anomalous terms ($V = \Delta = 0$), we have that $\mathcal{C} = 1/3$. For the Kitaev chain ($V = 0$, $\Delta \neq 0$), however, we have that $\mathcal{C} = 1/6$ because the central charge takes half the value of the homogeneous chain. For $\Delta = 0$ and $V \neq 0$, the $\mathcal{C} = 1/3$ scaling was found to hold for V within the extended phase [45] in the half-filled Aubry-André model. However, Ref. [47] found regimes where $\mathcal{C}$ was smaller even for electron fillings within the extended phase for a long-range Aubry-André model, in the presence of multifractal to extended mobility edges. In the localized phase, S only grows logarithmically for $N_A \lesssim \xi$, where ξ is the localization length [45,47,48]. At critical points containing multifractal eigenstates, S was found to still scale logarithmically with N_A, although with significantly smaller $\mathcal{C}$, accompanied by possible log-periodic oscillations [55], as previously observed for aperiodic quantum spin chains [56,57].

We will also compute the ground state fidelity, defined as [58,59]

$$F(\Psi(\lambda), \Psi(\lambda')) = |\langle\Psi(\lambda)\rangle\, \Psi(\lambda')|, \tag{7}$$

where $|\Psi(\lambda)\rangle$ is the system's ground-state and λ is some selected parameter of the model. In the case of noninteracting fermions, the overlap in Eq. (7) can be simply computed through $F(\Psi(\lambda), \Psi(\lambda')) = |\det(\mathbf{\Phi}_\lambda^\dagger \mathbf{\Phi}_{\lambda'})|$, where $\mathbf{\Phi}_\lambda$ is a $N \times M$ matrix containing the M filled single-particle eigenstates in its columns. Taking $\lambda' = \lambda + \delta\lambda$, we can compute the leading-order term of the fidelity as $\delta\lambda \to 0$. This term corresponds to the fidelity susceptibility χ_F, which can be defined as [59,60]

$$\chi_F = -\frac{\partial^2 F}{\partial(\delta\lambda)^2} = \lim_{\delta\lambda\to 0}\frac{-2\log F}{(\delta\lambda)^2}. \tag{8}$$

In the following, we choose $\delta\lambda$ small enough for χ_F to be converged. The finite-size scaling of χ_F can be used to tackle critical points and critical exponents. At a critical point, the maximum of χ_F, typically scales super extensively and its maximizant approaches the critical point as the system size is increased [59].

C. Localization probes

To inspect the localization properties, we compute inverse participation ratios (IPR). For each single-particle eigenstate $|\psi_\alpha\rangle = \sum_n \psi_n^\alpha |n\rangle$, where $\{|n\rangle\}$ is a basis localized at each site (or the Nambu basis for $\Delta \neq 0$), the generalized IPR is given by $\mathrm{IPR}_\alpha(q) = (\sum_n |\psi_n^\alpha|^2)^{-q}\sum_n |\psi_n^\alpha|^{2q}$ [61]. In general, we have $\mathrm{IPR}_\alpha(q) \sim N^{-\tau(q)}$, where $\tau(q) = D_r(q)(q-1)$. In the extended phase, we have $D_r(q) = D$, while in the localized phase the IPRs become L-independent for L sufficiently larger than the localization length and therefore $D_r(q) = 0$. Critical points/phases in 1D quasiperiodic systems have multifractal eigenstates, in which case $D_r(q)$ is a nonlinear function of q. For the quasiperiodic Kitaev chain, we also define a momentum space generalized IPR. In the diagonal basis defined as $\gamma_\alpha = \sum_i u_{\alpha,i} c_i^\dagger + v_{\alpha,i} c_i$, we define $\tilde{u}_{\alpha,k} = L^{-1/2}\sum_j e^{2\pi jk/L} u_{\alpha,i}$ and $\tilde{v}_{\alpha,k} = L^{-1/2}\sum_j e^{2\pi jk/L} v_{\alpha,i}$. The momentum-space generalized IPR is then given by $\mathrm{IPR}_k(q) = \sum_k (|\tilde{u}_{\alpha,k}|^{2q} + |\tilde{v}_{\alpha,k}|^{2q}) \sim L^{-\tau_k(q)}$. In this case, we have $\tau_k(q) = D_k(q)(q-1)$, with $D_k(q) = 0$ for ballistic extended states, $D_k(q) = 1$ for localized states and $D_k(q)$ is again a nonlinear function of q for multifractal states. In what follows, we mostly compute the real-space IPR and set $q = 2$, unless otherwise stated, defining $\mathrm{IPR} = \mathrm{IPR}(q = 2)$.

D. Topological invariant

Finally, to inspect topological properties of the quasiperiodic Kitaev chain, we make use of the topological invariant introduced in Ref. [51]. By writing the Hamiltonian in terms of two species of Majorana fermions, the equations of motion for zero energy Majorana modes can be written in terms of transfer matrices (see Appendix B for details). The transfer matrix for one of the species of modes is defined, for a system of length N, as $\mathrm{A}_N = \prod_{n=1}^N A_n$, where $A_n^{ij} = V_n/(\Delta + t)\delta_{i,0}\delta_{j,0} + (\Delta - t)/(\Delta + t)\delta_{i,0}\delta_{j,1} + \delta_{i,1}\delta_{j,0}$. For the other species, the transfer matrix is $B_n = \sigma_x A_n^{-1}\sigma_x$. A topological invariant can then be defined as in Ref. [51],

$$\nu_T = -(-1)^{n_f}, \tag{9}$$

where n_f is the number of eigenvalues of A_N with magnitude smaller than unity. Inside a topological phase $\nu_T = -1 (n_f = 0, 2)$, while in a trivial phase $\nu_T = 1 (n_f = 1)$.

E. Structure factor

To compare the results for the entanglement entropy scaling with other physical observables, we also compute the momentum structure factor, defined as

$$\mathcal{S}(q) = N^{-1}\sum_{j,l}[\langle n_j n_l\rangle - \langle n_j\rangle\langle n_l\rangle]e^{iq(j-l)}. \tag{10}$$

In the noninteracting limit, $\mathcal{S}(q)$ can be computed through

$$\mathcal{S}(q) = \frac{1}{N}\sum_{i,j=1}^{N}[\langle c_i^\dagger c_j\rangle\delta_{ij} - \langle c_i^\dagger c_j\rangle\langle c_j^\dagger c_i\rangle + \langle c_i^\dagger c_j^\dagger\rangle\langle c_j c_i\rangle]e^{iq(i-j)}, \tag{11}$$

where all these single-particle correlation functions can be computed at once through the correlation matrix $\boldsymbol{\chi}$ defined above. In gapless extended phases, $\mathcal{S}(q)$ typically behaves as $\mathcal{S}(q) = \frac{K}{2\pi}q$ at small q [62].

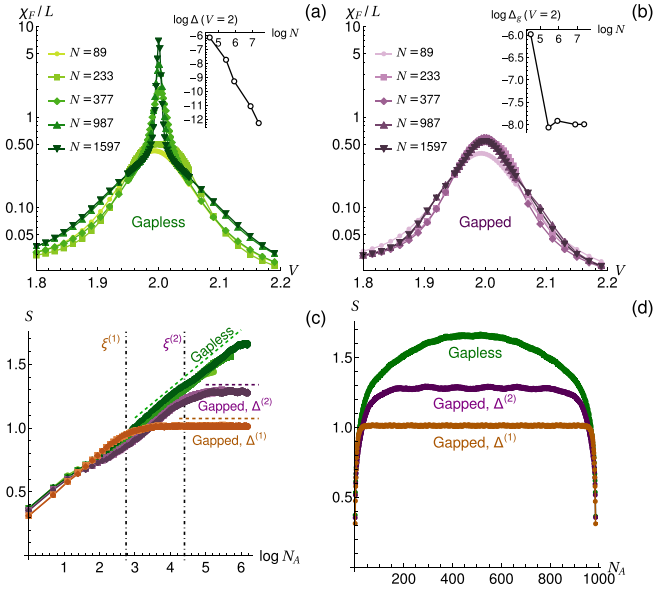

FIG. 1. Results for the Aubry-André model. (a), (b) χ_F/L at fillings $\rho = 1/4$ (a) and $\rho =$ mod $(57\tau, 1)$ (b), for fixed twist $\kappa = 1.7$ and $\phi = 1.123/N$. The insets show the energy gap as a function of system size for $V = 2$. (c) Entanglement entropy as function of $\log N_A$ up to $N_A = N/2$ for $V = 2$, for $\rho = 1/4$ (green), $\rho^{(1)} =$ mod $(10\tau, 1)$ (orange), and $\rho^{(2)} =$ mod $(57\tau, 1)$ (purple), and for system sizes $N = \{377, 610, 987\}$ (respectively, from lighter to darker color shade). Averages over $N_c = 1800$ configurations were made. (d) Entanglement entropy for $N_A \in [1, N]$, for $N = 987$, for the same parameters as in panel (c).

III. RESULTS

A. Aubry-André and GPS models

We start by analyzing the Aubry-André model. Some care is needed when computing the entanglement entropy, since energy gaps are known to open at commensurate fillings $\rho_n =$ mod $(n\tau, 1)$, $n \in \mathbb{Z}$ [63,64]. In fact, by applying perturbation theory in the quasiperiodic potential with respect to the homogeneous system, one finds that a gap is opened at filling ρ_n at order $|n|$ in perturbation theory and therefore the gap size typically decreases with $|n|$. While in the extended phase, gaps can only be effectively opened for $|n| \lesssim \xi$, where ξ is the correlation length ($\xi = 1/\log(2/V)$ in the extended phase for the Aubry-André model [12]), at critical points/phases ξ diverges and gaps can open at any order. For a finite system, we cannot get arbitrarily close to an incommensurate filling and we may end up choosing a (gapped) commensurate filling for some sizes. To try to avoid this problem we (i) start by choosing a number $N_p' = \lfloor \rho N \rceil$ of filled states, where $\lfloor x \rceil$ rounds x to the nearest integer; (ii) compute the energy gaps $\Delta_g^0 = \epsilon(N_p') - \epsilon(N_p' - 1)$ and $\Delta_g^1 = \epsilon(N_p' + 1) - \epsilon(N_p')$, where $\epsilon(N_p)$ is the single-particle eigenenergy of the N_pth eigenstate, and choose the final number of filled states to be $N_p = N_p' - 1 + \arg\min_j\{\Delta_g^j\}$, $j = 0, 1$. In this way, by always choosing the smallest gap closer to the chosen filling ρ we minimize the risk of accidentally coming across a commensurate filling for a given system. In Fig. 1 we show the results for the fidelity susceptibility and entanglement entropy obtained by carrying out the procedure just described for the Aubry-André model, at quarter-filling ($\rho = 1/4$), comparing with the results for a close commensurate filling $\rho_{57} =$ mod $(57\tau, 1) \approx 0.228$. In Fig. 1(a) we find true criticality since χ_F is superextensive at the critical point. This arises from the gapless nature of the chosen filling, as can be seen by the decreasing of the energy gap, Δ_g, with N at the critical point [inset of Fig. 1(a)]. For the commensurate filling, the system is gapped as can be seen by the convergence of Δ_g in N, in the inset of Fig. 1(b). Even though this gap is quite small, we can see that there is clearly no divergence in χ_F/N for a sufficiently large system size at the critical point. In this case, the system is always gapped, even at the critical point, which gives rise to an avoided criticality. These qualitative differences naturally manifest in the scaling of the entanglement entropy, as shown in Figs. 1(c) and 1(d). While in the gapless case, it scales as $\log N_A$ for $N_A \ll N$, only saturating at extensively larger length scales $\Lambda \simeq N/2$ [see Eq. (6)], in the gapped case, it only grows up to a N-independent length scale ξ_g, inversely proportional to the gap size. In Figs. 1(c) and 1(d) we also compare the results for fillings $\rho^{(1)} = \rho_{10}$ and $\rho^{(2)} = \rho_{57}$, where we clearly see that S saturates for $N_A \gtrsim \xi_g^{(1)}$ and $N_A \gtrsim \xi_g^{(2)} > \xi_g^{(1)}$ since $\Delta^{(1)} > \Delta^{(2)}$.

From this point on we focus on incommensurate/gapless fillings. In Fig. 2(a) we compute the entanglement entropy for the quarter-filled Aubry-André model, and for V close to the critical point. At the critical point we see that S scales as $\log N_A$ with $\mathcal{C} \approx 0.23$, slower than in the homogeneous system. Interestingly, close to the critical point we see that S closely follows the critical behavior for length scales $N_A \lesssim \xi$, where ξ is the correlation length ($\xi = 1/\log(2/V)$ in the extended phase, while $\xi = 1/\log(V/2)$ in the localized phase). For $N_A \gtrsim \xi$, we see a crossover to a scaling with $\mathcal{C} = 1/3$ in the extended phase, as in the homogeneous case, while there is a saturation in the localized phase. In Fig. 2(b), we compute the scaling of S in different critical points/phases of the GPS model, comparing with the results obtained deep in the extended phase. We see that the scaling of S in the critical phase can vary significantly, and even closely resemble the homogeneous/extended scaling. This is in contrast with previous results obtained for the Aubry-André model with long-range hoppings for which $\mathcal{C}$ was always found to be significantly lower than in the homogeneous or extended case, when the fillings were chosen in regions of multifractal eigenstates. We also note that even though S grows with $\log N_A$, it also shows small oscillations. These oscillations are expected: in fact log-periodic oscillations were previously found at the critical point of the half-filled Aubry-André model with $\tau = 1/\sqrt{2}$ [55] and also in aperiodic spin chains [56,57]. In Figs. 2(c) and 2(d), we compute $\mathcal{C}$ at localization-delocalization transitions [Fig. 2(c)] and inside the critical phase [Fig. 2(d)] by fitting $S(N_A)$ to Eq. (6). We find that $\mathcal{C}$ can take a wide range of nonuniversal values. Interestingly, for localization-delocalization transitions at filling $\rho = 1/4$ we find that the scaling of the entanglement entropy for the Aubry-André and GPS models is compatible, in agreement with the critical point universality proposed in Ref. [55]. This again suggests that at extended-localized transitions the behavior of entanglement entropy is universal for significantly different models at fixed fillings, as conjectured in Ref. [55].

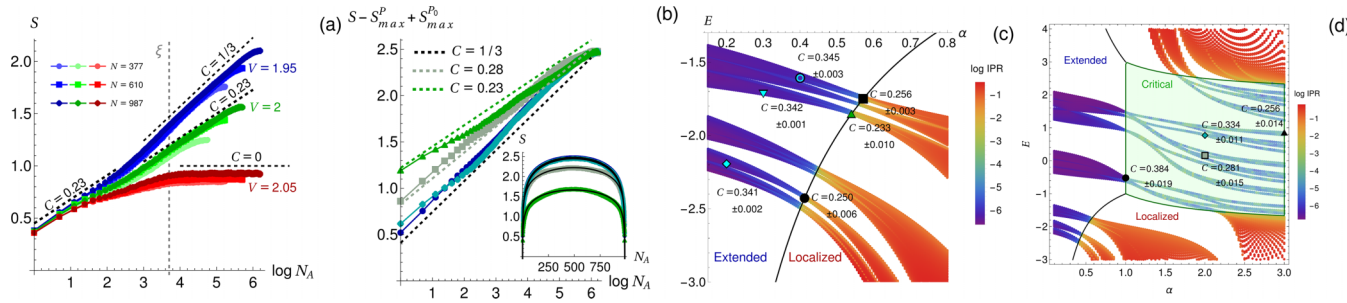

FIG. 2. (a) Entanglement entropy S for the Aubry-André model, for filling $\rho = 1/4$. The blue, green and red data points correspond to $V = 1.95$ (extended), $V = 2$ (critical) and $V = 2.05$ (localized), respectively. The dashed lines are guides to the eye for the scaling of the entanglement entropy. The gray dashed line indicates $\log \xi = 2.7$, where ξ is approximately the exact correlation length for $V = 1.95$ ($\xi = 1/\log 2/V$) and $V = 2$ ($\xi = 1/\log V/2$). (b)–(d) Results for the GPS model. (b) S for different critical points [$V = 1, \alpha = 2, \rho = 0.47$ (green); $V = 1, \alpha = 2, \rho = 0.538$ (light blue); $V = 1, \alpha = 0.539, \rho = 0.25$ (gray)] and an extended point ($\rho = 0.25, \alpha = 0, V = 1$). S was shifted so that the maxima coincide for all the analyzed points, where P_0 is the extended point and P is the point being analyzed. These points are signaled in panels (c), (d), with the plot markers matching the ones in this figure. The dashed lines show the slopes $\mathcal{C}$ obtained by fitting S to Eq. (6) for all N_A, where the fits are shown in the inset. (c) IPR for the GPS model around an extended-to-localized transition, for $L = 987$ and $V = 1$, along with fitting results for $\mathcal{C}$ at different points. The black line denotes the analytical mobility edge between the extended and localized phases. (d) IPR for the same model, in a range of parameters containing the critical phase, together with the value of $\mathcal{C}$ extracted from the fit within this phase. The error bars correspond to the standard deviation of mean between the fitted $\mathcal{C}$ for the three larger considered sizes, $N = \{610, 987, 1597\}$. For all the calculations of the entanglement entropy in panels (a)–(d), we averaged over 1800 configurations of shifts and twists for $N = \{377, 610, 987\}$ and 252 configurations for $N = 1597$.

We now try to establish a connection between the scaling of S and other physical properties. At critical points, correlation functions of the type $\langle \mathcal{O}_i \mathcal{O}_j \rangle$ are expected to decay in a power-law fashion as $\langle \mathcal{O}_i \mathcal{O}_{i+\epsilon} \rangle \sim |\epsilon|^{-y_\mathcal{O}}$ for large enough $|\epsilon|$. Taking the simplest correlation function, $\langle c_i^\dagger c_{i+\epsilon} \rangle$, we find that $\langle c_i^\dagger c_{i+\epsilon} \rangle \sim |\epsilon|^{-1}$ in the extended phase with the interesting possible formation of moiré patterns (see Appendix B); while in the localized phase $\langle c_i^\dagger c_{i+\epsilon} \rangle \sim e^{-|\epsilon|/\xi}$, where ξ is the localization length. At critical phases/points, however, there are very large fluctuations as function of ϵ and it becomes challenging to define the power-law exponent. In fact, the scaling of the maxima of these fluctuations is compatible with $|\epsilon|^{-1}$. Therefore, no significant distinctions in the scalings of $g_r(\epsilon)$ were found in the critical regions. The connection between S and the general behavior of correlation functions is therefore more subtle. In fact, a clear relation between the entanglement entropy and the low-momentum scaling of the structure factor $\mathcal{S}(q)$, given in Eq. (10), can be found. In Fig. 3(a) we can see that only the slope of the scaling, K [see below Eq. (10)], changes at critical points, while the linear scaling in q still holds as in the extended phase, up to small oscillations. By computing K for the different critical and extended points that we studied in Fig. 2, and comparing the results with $\mathcal{C}$, we verified that K increases with $\mathcal{C}$ as shown in Fig. 3(b). While at extended points we have $K \approx 1$ (blue points in Fig. 3) as in the homogeneous case, in the critical case the values of K can vary significantly.

B. Quasiperiodic Kitaev chain

The quasiperiodic Kitaev chain has a well-known phase diagram in the $\Delta - V$ plane for $\mu = 0$ [33], shown in the inset of Fig. 4 (see also Ref. [35] for full localization phase diagram and Ref. [65] for exact analytical solution). Here we computed the entanglement entropy at the critical line of the transition between a topological phase with critical eigenstates, having majorana zero modes, and a trivial localized phase. The results for $\mathcal{C}$ are shown in Figs. 4(a) and 4(b). For $(V, \Delta) = (2, 0)$, $\mathcal{C}$ has the value of the Aubry-André critical point ($\mathcal{C} \approx 0.26$ at half-filling [45]). However, for finite Δ, $\mathcal{C}$ quickly becomes smaller, getting close to the homogeneous Kitaev chain's value, $\mathcal{C} = 1/6$, with the most significant deviations arising only at small N_A. This can be observed by fitting the scaling of the entanglement entropy at small N_A across the critical line—Fig. 4(b)—for which we see a significant V- or Δ-dependence. When fitting S to Eq. (6) using all N_A, we found that $\mathcal{C}$ is essentially constant for different critical points of the transition, in contrast to the critical points of the unpaired models, for which $\mathcal{C}$ varied significantly. In Fig. 4(c)

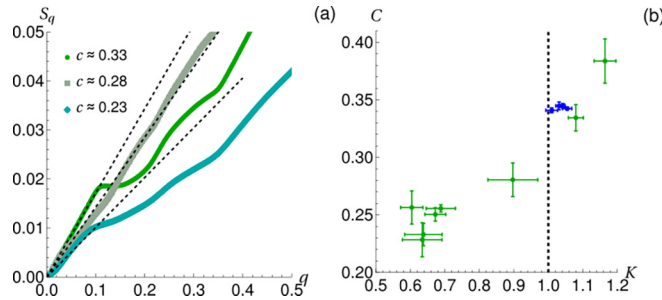

FIG. 3. (a) Structure factor $\mathcal{S}(q)$ for the same critical points analyzed in Fig. 2, with the corresponding values of $\mathcal{C}$ indicated in the legend. The black dashed lines correspond to the $\mathcal{S}(q) = Kq/(2\pi)$, with the K computed in panel (b) for the corresponding critical point. (b) $\mathcal{C}$ vs K for the different critical (green) and extended (blue) points studied in Fig. 2. K was computed through $K = 2\pi \mathcal{S}(\delta q)/\delta q$, with $\delta q = 20\pi/N$ and for a fixed random configuration of κ and ϕ (the results of $\mathcal{S}(q)$ depend very weakly on κ and ϕ). The error bars correspond to the standard deviation of the obtained results for the system sizes $N = \{1597, 2584, 4181\}$. The extended points are clustered close to $K = 1$, marked with the vertical dashed line.

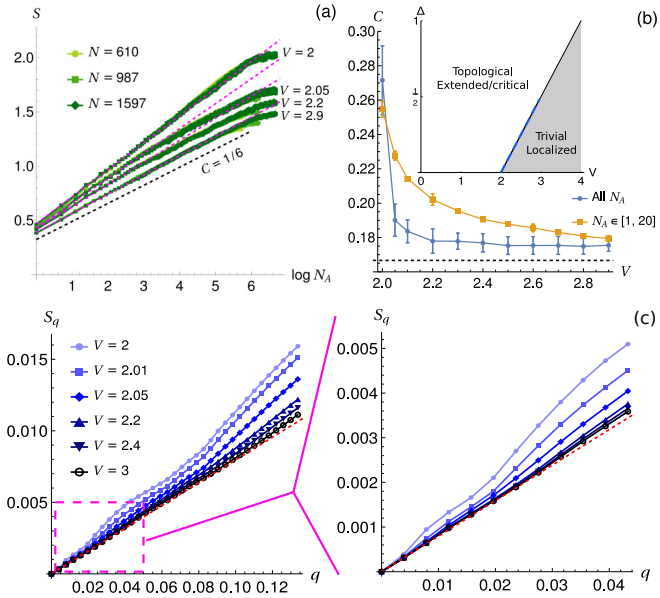

FIG. 4. (a) S for the quasiperiodic Kitaev chain, for $\mu = 0$ and different (V, Δ) across the topological transition shown in the inset of panel (b), given by $\Delta(V) = V/2 - 1$. The values of V are indicated close to the corresponding curves. The dashed magenta lines correspond to linear fits made for $N_A \leqslant 20$. (b) $\mathcal{C}$ obtained by fitting S to Eq. (6) for all N_A (blue) and by making a linear fit of the $(\log N_A, S)$ data only for $N_A \leqslant 20$ (yellow). The data points were computed by averaging the results obtained for the system sizes $N = \{610, 987, 1597\}$ and the error bars correspond to the standard deviation. The inset contains the topological phase diagram in the (V, Δ) plane. The blue dashed line in the inset indicates the explored range of the critical line. (c) Structure factor $\mathcal{S}(q)$ for $N = 1597$, a random ϕ and for different V along the critical line shown in the inset of (b). In the right figure we show a close-up of the results at smaller q. The red dashed line corresponds to $\mathcal{S}(q) = Kq/(2\pi)$ with $K = 1/2$.

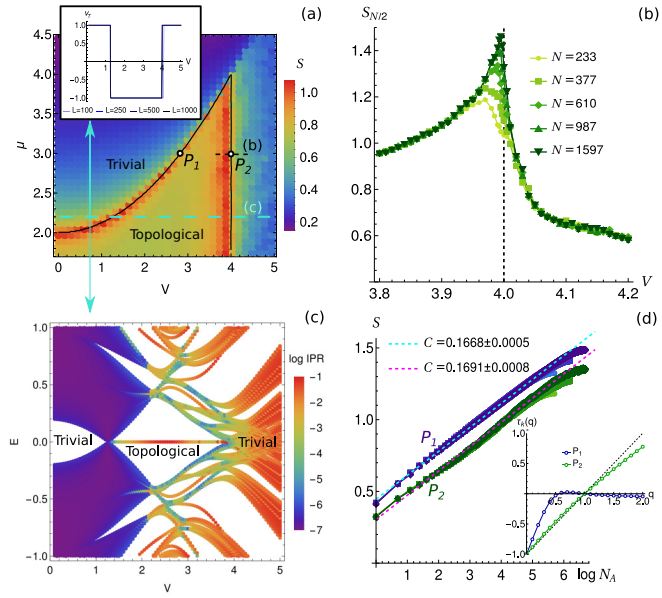

FIG. 5. Results for $\Delta = 1$. (a) S for $N = 233$ and $N_A = [N/6]$, with each point corresponding to an average over 75 realizations. The full black line shows the phase boundaries obtained through the topological invariant in Eq. (9). The inset show the results for this topological invariant at a fixed μ cut ($\mu = 2.2$) marked by the cyan dashed line. (b) Finite-size scaling of S for variable N and $N_A = [N/2]$. We averaged over $N_c = 1800$ configurations for $N \leqslant 987$ and $N_c = 252$ for $N = 1597$. (c) IPR results for $N = 987$, with open boundary conditions, and for parameters at the cyan dashed cut in panel (a). (d) S at critical points P_1 and P_2 indicated in panel (a). The lighter, intermediate and darker colors correspond, respectively, to $N = 610, 987, 1597$, with the results respectively averaged over $N_c = 1800, 1800, 252$ configurations. The inset contains the results for the multifractal exponent $\tau_k(q)$, computed by fitting $\mathrm{IPR}_k(q)$ for $N \in [144, 2584]$. We used $N_c \in [25 - 725]$ configurations of ϕ for P_2 and a single random configuration for P_1 (the ϕ-dependence is negligible in this case). We note that for P_1, $\tau_k(q)$ deviates significantly from 0 for small q, which we attribute to finite-size effects.

we show results for the structure factor $\mathcal{S}(q)$ along the critical line. We see that for any finite Δ ($V > 2$), the small-q behavior of the structure factor follows the expected behavior of the homogeneous Kitaev chain—$\mathcal{S}(q) = Kq/(2\pi)$ with $K = 1/2$. Deviations from this behavior are observed for larger q the larger the Δ. This perfectly correlates with the results of the entanglement entropy, where deviations from the homogeneous behavior only occur up to length scales that decrease with Δ.

To understand whether the almost constant value of $\mathcal{C}$ was a special feature of the analyzed transition, we also studied the $\mu \neq 0$ case. In this case we can have reentrant topological transitions, similar to what is observed for topological Anderson insulators, in the disordered case [66,67]. This is shown in Fig. 5(a) for $\Delta = 1$. In this figure, we can see that we can start in a trivial phase, at $\mu > 2$, and transition into a topological phase by increasing V. The topological phase contains zero-energy modes as expected, which we illustrate in Fig. 5(c). At an even larger value of V, we have a new topological transition back into a trivial phase. These two topological transitions are however of different nature in terms of localization properties. Exactly at the transition point the eigenstates are ballistic in the first and multifractal in the second. This is shown in the inset of Fig. 5(d), where we plotted $\tau_k(q)$ for examples of these transitions, at points P_1 and P_2, indicated in Fig. 5(a). We can see, however, that the scaling of the entanglement entropy is similar for both transitions, apart from the existence of oscillations in the critical case, as in the other studied critical points.

IV. DISCUSSION

In this work, we characterized in detail the entanglement entropy in different models of one-dimensional fermionic quasiperiodic systems, focusing on multifractal critical points/phases. In the absence of pairing, we found that the entanglement entropy follows the expected behavior for one-dimensional critical systems, but can show possible small oscillations. Similar log-periodic oscillations were previously found in Refs. [56,57] for aperiodic spin chains and in Ref. [55] both for the noninteracting and interacting Aubry-André model. In the absence of pairing, we found that the characteristic coefficient $\mathcal{C}$ that governs the scaling

of the entanglement entropy with subsystem size N_A and total size N depends significantly on the model parameters and electron filling. At some critical points, we observed that the entanglement entropy even behaves similarly to the homogeneous case, with $\mathcal{C} \approx 1/3$. This is in contrast with previous studies where $\mathcal{C}$ was always found to be significantly smaller at critical multifractal phases/points, compared to the homogeneous case [45,47]. Although there are significant variations of $\mathcal{C}$, we find that compatible values are obtained for the Aubry-André and GPS models at critical points of localization-delocalization transitions, for a fixed filling. This is in agreement with Ref. [55], where a universal behavior of the entanglement entropy was found at the localization transitions of different half-filled quasiperiodic chains. We also compared the behavior of the entanglement entropy with correlation functions and found that $\mathcal{C}$ was closely related with the long-wavelength behavior of the momentum structure factor.

For critical quasiperiodic Kitaev chains, we found that the addition of even small pairing terms is highly relevant for the behavior of the entanglement entropy. Independently of studied critical points, we find that it behaves similarly to the homogeneous critical Kitaev chain, where $\mathcal{C} = 1/6$, departing from the nonuniversal larger values of $\mathcal{C}$ computed in the unpaired case. The most significant deviations from $\mathcal{C} = 1/6$ only occur at small length scales. In very good agreement with these results, the small momentum behavior of the structure factor also follows the expected behavior of the homogeneous Kitaev chain, with deviations only arising at larger momenta. The topological nature of the quasiperiodic Kitaev transition may be behind the resilience of the entanglement entropy and structure factor behaviors for the analyzed critical points.

Future interesting studies include to address the impact of interactions on the entanglement entropy, in critical phases with multifractal eigenstates. In Ref. [55], short-range spinless interactions were found to be irrelevant at critical points between extended and localized phases, so we expect that our results at these transitions also hold in the interacting case. However, interactions can be relevant in multifractal critical phases of quasiperiodic systems [68], which may change the behavior of the entanglement entropy.

ACKNOWLEDGMENTS

The author acknowledges support from FCT-Portugal through the Grant No. SFRH/BD/145152/2019. The author also acknowledges partial support from Fundação para a Ciência e Tecnologia (FCTPortugal) through Grant No. UID/CTM/04540/2019 and Grant No. UIDB/04650/2020. We finally acknowledge the Tianhe-2JK cluster at the Beijing Computational Science Research Center (CSRC) and the OBLIVION supercomputer, through projects HPCUE/A1/468700/2021, 2022.15834.CPCA.A1, and 2022.15910.CPCA.A1 (based at the High Performance Computing Center - University of Évora) funded by the ENGAGE SKA Research Infrastructure (Reference No. POCI-01-0145-FEDER-022217 - COMPETE 2020 and the Foundation for Science and Technology, Portugal) and by the BigData@UE project (Reference No. ALT20-03-0246-FEDER-000033 - FEDER and the Alentejo 2020 Regional Operational Program. Computer assistance was provided by CSRC's and OBLIVION's support teams.

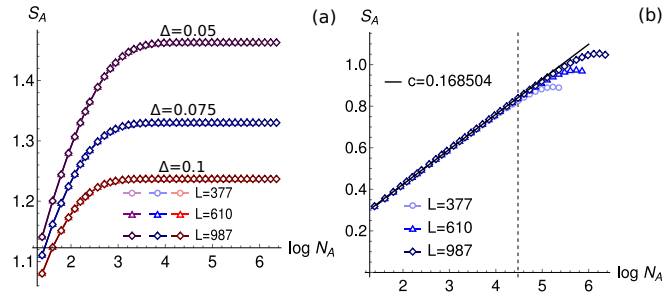

FIG. 6. (a) Entanglement entropy for the homogeneous Kitaev chain, for $\mu = 0$ and variable Δ. Note that the energy gap increases with Δ. Therefore, for larger Δ, S saturates for smaller N_A, of the order of the inverse gap. (b) Entanglement entropy for the clean Kitaev chain, for $\Delta = 0.1$, $\mu = 2$ (critical point). S_A scales with the correct pre-factor $\mathcal{C} \approx 1/6$ consistent with the central charge $c = 1/2$ of the Kitaev model.

APPENDIX A: QUASIPERIODIC KITAEV CHAIN: CLEAN LIMIT AND TOPOLOGICAL PROPERTIES

In this Appendix, we provide additional details on how the topological properties of the quasiperiodic Kitaev chain were studied in the main text. For $V = 0$, this model is homogeneous and exhibits a phase transition at $|\mu| = |t|$, for any Δ [51]. At this point, the entanglement entropy scales with $\mathcal{C} = 1/6$ [1]. Otherwise, the system is gapped and the entanglement entropy saturates for large enough N_A. We reproduce these results, in Fig. 6.

To study the topological properties of the model, in particular for the phase diagram in Fig. 5(a), we used a topological invariant first defined in Ref. [51]. We now provide some additional details on this quantity. Let us introduce the Majorana fermions a_n and b_n such that $c_n = (a_n + ib_n)/2$. a_n and b_n satisfy $\{a_n, b_n\} = 0$ and $\{a_n, a_m\} = \{b_n, b_m\} = 2\delta_{mn}$ (and therefore $a_n^2 = b_n^2 = 1$). The Hamiltonian for the quasiperiodic Kitaev chain becomes

$$H = \frac{i}{2}\sum_n ((-t+\Delta)a_n b_{n+1} + (t+\Delta)b_n a_{n+1} + [V\cos(2\pi\tau n + \phi) - \mu]a_n b_n) + \text{cte}. \quad \text{(A1)}$$

The Majorana zero modes are represented by the operators $\Gamma_a = \sum_n \alpha_n a_n$ and $\Gamma_b = \sum_n \beta_n b_n$, whose amplitudes α_n and β_n satisfy the zero-energy equations of motion for the Hamiltonian in Eq. (A1):

$$\begin{aligned}(t-\Delta)\alpha_{n-1} + (t+\Delta)\alpha_{n+1} - V_n\alpha_n = 0,\\ -(t+\Delta)\beta_{n-1} - (t-\Delta)\beta_{n+1} + V_n\beta_n = 0,\end{aligned} \quad \text{(A2)}$$

where $V_n = V\cos(2\pi\tau n + \phi) - \mu$. We can write these decoupled equations in the transfer matrix form:

$$\begin{pmatrix}\alpha_{n+1}\\ \alpha_n\end{pmatrix} = A_n\begin{pmatrix}\alpha_n\\ \alpha_{n-1}\end{pmatrix}, \quad A_n = \begin{pmatrix}\frac{V_n}{\Delta+t} & \frac{\Delta-t}{\Delta+t}\\ 1 & 0\end{pmatrix}, \quad \text{(A3)}$$

$$\begin{pmatrix}\beta_{n+1}\\ \beta_n\end{pmatrix} = B_n\begin{pmatrix}\beta_n\\ \beta_{n-1}\end{pmatrix}, \quad B_n = \sigma_x A_n^{-1}\sigma_x, \quad \text{(A4)}$$

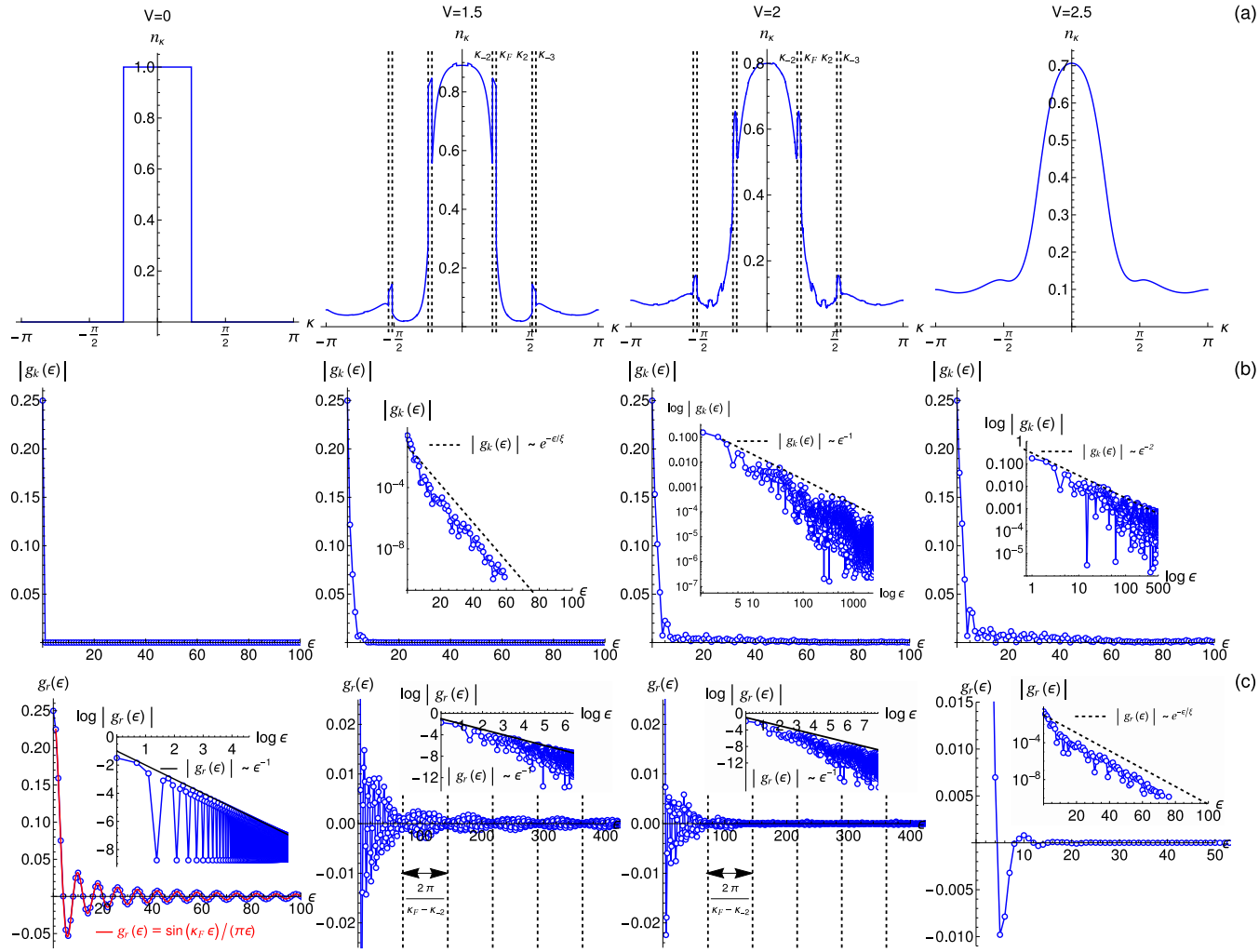

FIG. 7. Results for n_κ (a), $g_\kappa(\epsilon)$ (b), and $g_r(\epsilon)$ (c), for the quarter-filled Aubry-André model, for different values of V in each column (indicated above the corresponding column). In panel (a) we label some values $\kappa_n = \kappa_F + 2\pi\tau n$, $n \in \mathbb{Z}$. (b) The first inset from left to right is a log plot, showing that $g_\kappa(\epsilon)$ decays exponentially with ϵ for $V = 1.5$, with a exact correlation length $\xi = 1/\log(2/V)$, while the last two insets are log-log plots showing that $|g_\kappa(\epsilon)|$ decays as a power-law envelope for $V = 2$ and $V = 2.5$. (c) The red line in the leftmost figure corresponds to the exact result $g_r(\epsilon) = \sin(\kappa_F\epsilon)/(\pi\epsilon)$, for $V = 0$. The first three insets correspond to log-log plots showing the power-law envelop decay of $|g_r(\epsilon)|$, while the last plot is a log plot showing the exponential decay for $V = 2.5$ with the exact localization length $\xi = 1/\log(V/2)$. We note that there are moiré patterns that can be noted in the middle figures. These have a periodicity $\Delta\epsilon = 2\pi/(\kappa_F - \kappa_{-2})$, where κ_F is the Fermi momentum and κ_{-2} is indicated in panel (a). All the dashed/full lines in the insets are guides to the eye. The results are all for $N = 1597$, $\phi = 1.123$, $\kappa = 0.001$, except for $V = 2$ where we used $N = 4181$. A very small κ was used simply to break fermi-level degeneracies. Note that since this introduces a small imaginary part in $\chi_{rr'}$, we just took the real part of $g_r(\epsilon)$ in the figures.

where σ_x is a Pauli matrix. Considering a semi-infinite chain starting at site $n = 1$, we have $\alpha_0 = \beta_0 = 0$. At site $n = N + 1$ we have

$$\begin{pmatrix} \alpha_{N+1} \\ \alpha_N \end{pmatrix} = \mathcal{A}_L \begin{pmatrix} \alpha_1 \\ 0 \end{pmatrix}, \qquad \mathrm{A}_N = \prod_{n=1}^{N} A_n. \tag{A5}$$

In the same way, we can define

$$\mathrm{B}_N = \prod_{n=1}^{N} B_n. \tag{A6}$$

To have Majorana modes localized at the edges of the chain, both the eigenvalues of $\mathcal{A}_N$ should be either smaller or larger than one in magnitude as $N \to \infty$. In the former case, we have a localized a mode, while in the latter, we have a localized b mode (at the left boundary). If only one of the eigenvalues of $\mathcal{A}_N$ is larger than unity, then both the a and b modes are not normalizable and we cannot have localized Majorana modes.

Based on these considerations we can define a topological invariant as in Ref. [51]:

$$\nu_T = -(-1)^{n_f}, \tag{A7}$$

where n_f is the number of eigenvalues with magnitude smaller than unity. For $n_f = 0, 2$, $\nu_T = -1$ and the phase is topological. For $n_f = 1$, $\nu_T = 1$ and the phase is trivial.

APPENDIX B: SINGLE-PARTICLE CORRELATION MATRIX IN THE AUBRY-ANDRÉ MODEL

We finally provide additional results on single-particle correlation functions for the Aubry-André model. We define the real and momentum-space single-particle correlation matrices as

$$\chi_{rr'} = \langle c_r^\dagger c_{r'} \rangle, \tag{B1}$$

$$\Lambda_{\kappa\kappa'} = \frac{1}{N} \sum_{rr'} e^{\mathrm{i}(\kappa r - \kappa' r')} \chi_{rr'}. \tag{B2}$$

For translational invariant systems, $\Lambda_{\kappa\kappa'}$ is diagonal. In fact, we have $n_\kappa \equiv \Lambda_{\kappa\kappa} = \Theta[-(\kappa - \kappa_F)] - \Theta[-(\kappa + \kappa_F)]$, where κ_F is the Fermi momentum. An interesting question is what happens to $\Lambda_{\kappa\kappa'}$ when we switch on the quasiperiodic perturbation. On the one hand, gaps will open and n_κ will stop being the Heaviside function. On the other hand, off-diagonal elements appear in $\Lambda_{\kappa\kappa'}$ because translational invariance is broken.

We take the Aubry-André model as an example. For the Aubry-André model, different momenta are coupled if $\kappa - \kappa' = 2\pi\tau j,\ j \in \mathbb{Z}$, or, for a commensurate approximant with $\tau_c^n = F_{n-1}/F_n$, if $\kappa - \kappa' = 2\pi\tau_c^n j,\ j = 0, \ldots, N-1$ [12]. Therefore, it is convenient to use $\kappa_j = 2\pi\tau_c^n j$ and $\kappa'_j = 2\pi\tau_c^n j'$, with $j, j' = 0, \ldots, N-1$ and define

$$\Lambda_{jj'} = \frac{1}{N} \sum_{rr'} e^{i2\pi\tau_c^n (jr - j'r')} \chi_{rr'}. \tag{B3}$$

Note that due to periodic boundary conditions, $\Lambda_{j+mN, j'+lN} = \Lambda_{jj'}$ for $m, l \in \mathbb{Z}$. To have an idea on how $\Lambda_{jj'}$ behaves for $j \neq j'$, we define

$$g_\kappa(\epsilon) = \frac{1}{N} \sum_j \Lambda_{j,j+\epsilon}. \tag{B4}$$

For $\epsilon = 0$, we have that $g(0) = \mathrm{Tr}(|\mathbf{\Lambda}|) = \nu$, where ν is the filling. We define an analogous quantity for the real-space correlation function:

$$g_r(\epsilon) = \frac{1}{N} \sum_r \chi_{r,r+\epsilon}. \tag{B5}$$

We provide a summary of the results in Fig. 7, for the quarter-filled Aubry-André model. For $V = 0$, states with definite crystal momentum κ form the eigenbasis of the Hamiltonian and therefore $\Lambda_{\kappa\kappa'}$ is a diagonal matrix [which can be seen from the results for $g_\kappa(\epsilon)$], with $n_\kappa \equiv \Lambda_{\kappa\kappa} = \begin{cases} 1, & |\kappa| \leqslant \kappa_F \\ 0, & \text{otherwise} \end{cases}$. From this, one can easily obtain that $g_r(\epsilon) = \sin(\kappa_F \epsilon)/(\pi\epsilon),\ \epsilon > 0$. For $V > 0$ within the extended phase, we can see that $\Lambda_{\kappa\kappa'}$ is no longer diagonal, but $g_\kappa(\epsilon)$ decays exponentially away from the diagonal with a correlation length $\xi = 1/\log(2/V)$, the exactly known correlation length for the extended phase of the Aubry-André model. Furthermore, n_κ develops additional discontinuities at wave vectors $\kappa_n = \kappa_F + 2\pi\tau n, n \in \mathbb{Z}$, to which the Fermi momentum k_F couples in perturbation theory [63]. We note however that in practice, the coupling does not occur for any n due to the finite correlation length ξ: k_F does not effectively couple to k_n for $|n| \gg \xi$.

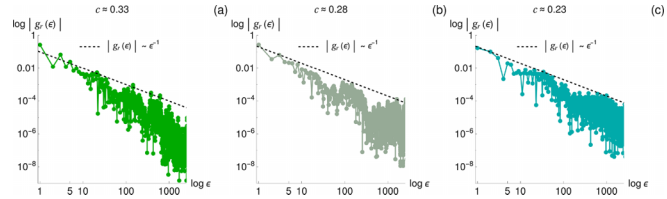

FIG. 8. $|g_r(\epsilon)|$ at the different critical points also considered in Fig. 2(b). In particular: (a) $V = 1, \alpha = 2, \rho = 0.47$; (b) $V = 1, \alpha = 2, \rho = 0.538$; (c) $V = 1, \alpha = 0.539, \rho = 0.25$. The computed entanglement entropy coefficient $\mathcal{C}$ is indicated above the figure of the corresponding critical point. The dashed black lines are guides to the eye corresponding to a $|g_r(\epsilon)| \sim \epsilon^{-1}$ scaling.

Even within the extended phase, curious situations can arise as we illustrate in Fig. 7 for the quarter-filled Aubry-André model. In this case there is a small-order κ_n corresponding to $n = -2$ very close to the Fermi momentum κ_F [69], which gives rise to the small momentum windows with large n_κ shown in Fig. 7(a). This translates in the formation of a real-space beating (moiré) pattern with wave vector $\Delta\kappa = \kappa_F - \kappa_{-2}$. This can be simply understood if one just considers the diagonal contributions of $\Lambda_{\kappa\kappa'}$, given by $\chi_{rr'} \approx N^{-1} \sum_\kappa e^{-\mathrm{i}\kappa(r-r')} n_\kappa$. Taking the large contributions at $\kappa \in [\kappa_{-2}, \kappa_F] \bigcup [-\kappa_F, -\kappa_{-2}]$, that we call $\chi_{rr'}^{(\Delta\kappa)}$, and assuming that they are approximately a constant $\tilde{n}_{\Delta\kappa}$, we get $\chi_{rr'}^{(\Delta\kappa)} \approx (2\pi)^{-1} \tilde{n}_{\Delta\kappa} (\int_{-\kappa_F}^{-\kappa_{-2}} + \int_{\kappa_{-2}}^{\kappa_F}) d\kappa e^{-\mathrm{i}\kappa(r-r')} \sim \cos[\kappa_F(r-r')] + \cos[\kappa_{-2}(r-r')]$, from which the beating effect seen in $g_r(\epsilon)$, in Fig. 7(c), is immediately captured. At the critical point $V = 2$, the correlation length diverges and the off-diagonal elements of $\Lambda_{\kappa\kappa'}$ start to decay in a power-law fashion, as can be seen from the results of $|g_\kappa(\epsilon)|$. In this case, the beating effect in $g_r(\epsilon)$ just mentioned becomes less obvious due to the more complex structure of the momentum-space correlation matrix. Interestingly, using the Aubry-André duality, one can easily check that the real- and momentum-space matrices $\chi_{rr'}$ and $\Lambda_{\kappa\kappa'}$ become equal at the critical point. Finally, in the localized phase, the off-diagonal elements of $\chi_{rr'}$ decay exponentially with the localization length $\xi = 1/\log(V/2)$, while the off-diagonal elements of $\Lambda_{\kappa\kappa'}$ decay with a power-law envelope.

From Fig. 7, we can see that the behavior of the real- and momentum-space correlation matrices at the critical point is highly nontrivial. In fact, we show in Fig. 8 that there is no clear distinction in the scaling of $g_r(\epsilon)$ for example critical points that have a significantly different scaling of the entanglement entropy $\mathcal{C}$.

[1] G. Vidal, J. I. Latorre, E. Rico, and A. Kitaev, Phys. Rev. Lett. **90**, 227902 (2003).
[2] P. Calabrese and J. Cardy, J. Stat. Mech.: Theory Exp. (2004) P06002.
[3] P. Calabrese and J. Cardy, J. Phys. A: Math. Theor. **42**, 504005 (2009).
[4] L. Amico, R. Fazio, A. Osterloh, and V. Vedral, Rev. Mod. Phys. **80**, 517 (2008).
[5] G. Refael and J. E. Moore, Phys. Rev. Lett. **93**, 260602 (2004).
[6] A. Saguia, M. S. Sarandy, B. Boechat, and M. A. Continentino, Phys. Rev. A **75**, 052329 (2007).
[7] G. Refael and J. E. Moore, J. Phys. A: Math. Theor. **42**, 504010 (2009).
[8] M. Pouranvari and K. Yang, Phys. Rev. B **89**, 115104 (2014).
[9] I. Mondragon-Shem and T. L. Hughes, Phys. Rev. B **90**, 104204 (2014).
[10] M. Pouranvari, Y. Zhang, and K. Yang, Adv. Conden. Matter Phys. **2015**, 397630 (2015).
[11] Y. Mohdeb, J. Vahedi, N. Moure, A. Roshani, H.-Y. Lee, R. N. Bhatt, S. Kettemann, and S. Haas, Phys. Rev. B **102**, 214201 (2020).
[12] S. Aubry and G. André, in *Proceedings of the VIII International Colloquium on Group-Theoretical Methods in Physics*, Annals of the Israel Physical Society, Vol. 3 (Hilger, Bristol, U.K., 1980).
[13] G. Roati, C. D'Errico, L. Fallani, M. Fattori, C. Fort, M. Zaccanti, G. Modugno, M. Modugno, and M. Inguscio, Nature (London) **453**, 895 (2008).
[14] Y. Lahini, R. Pugatch, F. Pozzi, M. Sorel, R. Morandotti, N. Davidson, and Y. Silberberg, Phys. Rev. Lett. **103**, 013901 (2009).
[15] M. Schreiber, S. S. Hodgman, P. Bordia, H. P. Lüschen, M. H. Fischer, R. Vosk, E. Altman, U. Schneider, and I. Bloch, Science **349**, 842 (2015).
[16] H. P. Lüschen, S. Scherg, T. Kohlert, M. Schreiber, P. Bordia, X. Li, S. Das Sarma, and I. Bloch, Phys. Rev. Lett. **120**, 160404 (2018).
[17] C. Huang, F. Ye, X. Chen, Y. V. Kartashov, V. V. Konotop, and L. Torner, Sci. Rep. **6**, 32546 (2016).
[18] J. H. Pixley, J. H. Wilson, D. A. Huse, and S. Gopalakrishnan, Phys. Rev. Lett. **120**, 207604 (2018).
[19] M. J. Park, H. S. Kim, and S. B. Lee, Phys. Rev. B **99**, 245401 (2019).
[20] B. Huang and W. V. Liu, Phys. Rev. B **100**, 144202 (2019).
[21] Y. Fu, E. J. König, J. H. Wilson, Y.-Z. Chou, and J. H. Pixley, npj Quantum Mater. **5**, 71 (2020).
[22] P. Wang, Y. Zheng, X. Chen, C. Huang, Y. V. Kartashov, L. Torner, V. V. Konotop, and F. Ye, Nature (London) **577**, 42 (2020).
[23] M. Gonçalves, H. Z. Olyaei, B. Amorim, R. Mondaini, P. Ribeiro, and E. V. Castro, 2D Mater. **9**, 011001 (2022).
[24] M. Pouranvari, Eur. Phys. J. B **96**, 48 (2023).
[25] Y. E. Kraus, Y. Lahini, Z. Ringel, M. Verbin, and O. Zilberberg, Phys. Rev. Lett. **109**, 106402 (2012).
[26] Y. E. Kraus and O. Zilberberg, Phys. Rev. Lett. **109**, 116404 (2012).
[27] M. Verbin, O. Zilberberg, Y. E. Kraus, Y. Lahini, and Y. Silberberg, Phys. Rev. Lett. **110**, 076403 (2013).
[28] D. J. Boers, B. Goedeke, D. Hinrichs, and M. Holthaus, Phys. Rev. A **75**, 063404 (2007).
[29] M. Modugno, New J. Phys. **11**, 033023 (2009).
[30] M. Verbin, O. Zilberberg, Y. Lahini, Y. E. Kraus, and Y. Silberberg, Phys. Rev. B **91**, 064201 (2015).
[31] L. Balents, C. R. Dean, D. K. Efetov, and A. F. Young, Nat. Phys. **16**, 725 (2020).
[32] E. Y. Andrei, D. K. Efetov, P. Jarillo-Herrero, A. H. MacDonald, K. F. Mak, T. Senthil, E. Tutuc, A. Yazdani, and A. F. Young, Nat. Rev. Mater. **6**, 201 (2021).
[33] W. DeGottardi, D. Sen, and S. Vishveshwara, Phys. Rev. Lett. **110**, 146404 (2013).
[34] F. Liu, S. Ghosh, and Y. D. Chong, Phys. Rev. B **91**, 014108 (2015).
[35] J. Wang, X.-J. Liu, G. Xianlong, and H. Hu, Phys. Rev. B **93**, 104504 (2016).
[36] X. Deng, S. Ray, S. Sinha, G. V. Shlyapnikov, and L. Santos, Phys. Rev. Lett. **123**, 025301 (2019).
[37] Y. Wang, L. Zhang, S. Niu, D. Yu, and X.-J. Liu, Phys. Rev. Lett. **125**, 073204 (2020).
[38] T. Čadež, R. Mondaini, and P. D. Sacramento, Phys. Rev. B **99**, 014301 (2019).
[39] T. Liu, X. Xia, S. Longhi, and L. Sanchez-Palencia, SciPost Phys. **12**, 027 (2022).
[40] M. Gonçalves, B. Amorim, E. V. Castro, and P. Ribeiro, Phys. Rev. Lett. **131**, 186303 (2023).
[41] X. Li, J. H. Pixley, D.-L. Deng, S. Ganeshan, and S. Das Sarma, Phys. Rev. B **93**, 184204 (2016).
[42] N. Roy and A. Sharma, Phys. Rev. B **100**, 195143 (2019).
[43] P. Ribeiro, M. Haque, and A. Lazarides, Phys. Rev. A **87**, 043635 (2013).
[44] M. Pouranvari, Phys. Rev. B **99**, 155121 (2019).
[45] G. H. Roósz, Z. Zimborás, and R. Juhász, Phys. Rev. B **102**, 064204 (2020).
[46] R. Ghosh and A. Das, Phys. Rev. B **103**, 024202 (2021).
[47] N. Roy and A. Sharma, Phys. Rev. B **103**, 075124 (2021).
[48] N. Roy and A. Sharma, Phys. Rev. B **97**, 125116 (2018).
[49] S. Ganeshan, J. H. Pixley, and S. Das Sarma, Phys. Rev. Lett. **114**, 146601 (2015).
[50] X. Cai, L.-J. Lang, S. Chen, and Y. Wang, Phys. Rev. Lett. **110**, 176403 (2013).
[51] W. DeGottardi, D. Sen, and S. Vishveshwara, New J. Phys. **13**, 065028 (2011).
[52] M. Y. Azbel, Phys. Rev. Lett. **43**, 1954 (1979).
[53] A. Szabó and U. Schneider, Phys. Rev. B **98**, 134201 (2018).
[54] Y. Wang, X. Xia, L. Zhang, H. Yao, S. Chen, J. You, Q. Zhou, and X. J. Liu, Phys. Rev. Lett. **125**, 196604 (2020).
[55] M. Gonçalves, J. H. Pixley, B. Amorim, E. V. Castro, and P. Ribeiro, Phys. Rev. B **109**, 014211 (2024).
[56] R. Juhász and Z. Zimborás, J. Stat. Mech.: Theory Exp. (2007) P04004.
[57] F. Igloi, R. Juhász, and Z. Zimborás, Europhys. Lett. **79**, 37001 (2007).
[58] P. Zanardi and N. Paunković, Phys. Rev. E **74**, 031123 (2006).
[59] S.-J. GU, Int. J. Mod. Phys. B **24**, 4371 (2010).
[60] W.-L. You, Y.-W. Li, and S.-J. Gu, Phys. Rev. E **76**, 022101 (2007).
[61] C. Aulbach, A. Wobst, G.-L. Ingold, P. Hänggi, and I. Varga, New J. Phys. **6**, 70 (2004).

[62] In a Luttinger liquid phase, K is the Luttinger liquid correlation parameter.
[63] B. Bernevig and T. Hughes, *Topological Insulators and Topological Superconductors* (Princeton University Press, Princeton, NJ, 2013).
[64] T. Cookmeyer, J. Motruk, and J. E. Moore, Phys. Rev. B **101**, 174203 (2020).
[65] M. Gonçalves, B. Amorim, E. V. Castro, and P. Ribeiro, Phys. Rev. B **108**, L100201 (2023).
[66] J. Li, R.-L. Chu, J. K. Jain, and S.-Q. Shen, Phys. Rev. Lett. **102**, 136806 (2009).
[67] L. Levy and M. Goldstein, Universe **5**, 33 (2019).
[68] M. Gonçalves, B. Amorim, F. Riche, E. V. Castro, and P. Ribeiro, arXiv:2305.03800.
[69] We note that even though κ_F is only well-defined for $V = 0$, n_κ still shows a sharp decrease at $\kappa = \kappa_F$ in the extended (and even critical) phase of the Aubry-André model.